

# High-Loading Poly(ethylene glycol)-Blended Poly(acrylic acid) Membranes for CO<sub>2</sub> Separation

Somi Yu, Seong Jin An, Ki Jung Kim, Jae Hun Lee,\* and Won Seok Chi\*

Cite This: *ACS Omega* 2023, 8, 2119–2127

Read Online

ACCESS |



Metrics &amp; More

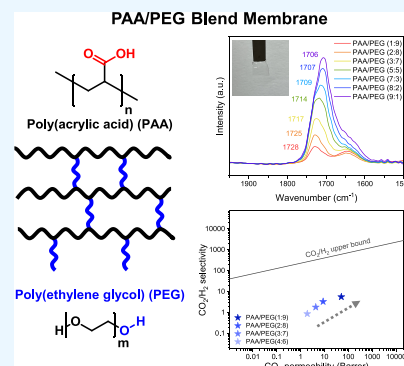


Article Recommendations



Supporting Information

**ABSTRACT:** Poly(ethylene glycol) (PEG) is an amorphous material of interest owing to its high CO<sub>2</sub> affinity and potential usage in CO<sub>2</sub> separation applications. However, amorphous PEG often has a low molecular weight, making it challenging to form into the membrane. The crystalline high average molar mass poly(ethylene oxide) (PEO) cannot exhibit CO<sub>2</sub> separation characteristics. Thus, it is crucial to employ low molecular weight PEG in high molecular weight polymers to increase the CO<sub>2</sub> affinity for CO<sub>2</sub> separation membranes. In this work, poly(acrylic acid) (PAA)/PEG blend membranes with a PEG-rich phase were simply fabricated by physical mixing with an ethanol solvent. The carbonyl group of the PAA and the hydroxyl group of the PEG formed a hydrogen bond. Furthermore, the thermal stability, glass transition temperature, and surface hydrophilicity of PAA/PEG blend membranes with various PEG concentrations were further characterized. The PAA/PEG(1:9) blend membrane exhibited an improved CO<sub>2</sub> permeability of 51 Barrer with high selectivities relative to the other gas species (H<sub>2</sub>, N<sub>2</sub>, and CH<sub>4</sub>; CO<sub>2</sub>/H<sub>2</sub> = 6, CO<sub>2</sub>/N<sub>2</sub> = 63, CO<sub>2</sub>/CH<sub>4</sub> = 21) at 35 °C and 150 psi owing to the enhanced CO<sub>2</sub> affinity with the amorphous PEG-rich phase. These PAA/PEG blend membrane permeation characteristics indicate a promising prospect for CO<sub>2</sub> capture applications.



## 1. INTRODUCTION

Carbon dioxide (CO<sub>2</sub>) is a major greenhouse gas that causes severe environmental issues including climate change and global warming.<sup>1,2</sup> Industrial fields, including energy, fossil fuel, transportation, and construction, contribute mostly to CO<sub>2</sub> emissions.<sup>1,2</sup> Additionally, a few separation processes require the removal of CO<sub>2</sub> to further purify the gas of interest. For example, CO<sub>2</sub> capture is required to stop CO<sub>2</sub> emissions from industrial flue gas systems (mainly CO<sub>2</sub>/N<sub>2</sub> mixture).<sup>3–5</sup> The natural gas sweetening process must produce highly purified CH<sub>4</sub> gas by removing a small amount of CO<sub>2</sub>.<sup>5,6</sup> The syngas process also purifies the H<sub>2</sub>/CO<sub>2</sub> gas mixture to generate pure H<sub>2</sub> gas as an energy source.<sup>5,7,8</sup> Thus, CO<sub>2</sub> is an impurity that requires a significant separation process scale to be removed from gas mixtures (e.g., CH<sub>4</sub>, N<sub>2</sub>, and H<sub>2</sub>).<sup>9</sup> Distillation, cryogenic separation, and absorption have been used to address the demand for CO<sub>2</sub> removal in gas mixtures.<sup>10,11</sup> However, the traditional separation processes require significant energy input, operation cost, and a large industrial module.<sup>12</sup> To address these issues, a membrane-based separation process has been proposed owing to its low operation cost and module compactness as well as the fact that it does not require heat-driven phase transition.<sup>12,13</sup>

The polymer-based membrane has been widely employed for gas separation because of its good processability, low cost, and ability to form a large-area thin film, which can significantly increase the gas flux for high productivity.<sup>3–6,14,15</sup> However, the polymer membrane generally shows a trade-off

relationship between permeability and selectivity.<sup>16</sup> This indicates that modifying the polymer structure to increase the permeability usually leads to a decrease in selectivity and *vice versa*. The upper bound limit, defined by Robeson, shows the empirically analyzed gas separation performance of interest based on state-of-the-art polymer membranes. This upper bound limit has been used to compare the separation performance of the developed membranes to describe the extent of the separation performance relative to recent transport data of polymer membranes in membrane science. The upper bound limit has been updated to reflect the discovery of new high-performance polymers developed with the aim of exceeding previously reported upper bounds.<sup>17,18</sup> To date, only a few commercially available polymer materials exist, such as cellulose acetate, polyimide, polysulfone, polycarbonate, and polydimethylsiloxane (PDMS). Thus, it is essential to develop polymer membranes to achieve high permeation and separation properties with material cost-effectiveness.<sup>19</sup>

Received: September 23, 2022

Accepted: December 21, 2022

Published: January 6, 2023



Poly(ethylene oxide) (PEO) and poly(ethylene glycol) (PEG), which both contain the polar ether segment that can form quadruple–quadruple interaction, have been widely used as CO<sub>2</sub> separation material candidates owing to their high CO<sub>2</sub> affinity.<sup>20–22</sup> However, high average molar mass PEO has significantly low gas separation properties due to its high crystallinity, which limits the polymer chain mobility.<sup>23–25</sup> Thus, harnessing the high average molar mass PEO has been challenging for CO<sub>2</sub> gas separation membrane application. On the other hand, low molecular weight PEG (non-crystalline PEO) is amorphous and has high chain mobility. Unfortunately, the low molecular weight PEG alone is liquid at room temperature, preventing the formation of a mechanically robust self-standing membrane for CO<sub>2</sub> gas separation. To effectively use low molecular weight PEG for CO<sub>2</sub> separation membranes, it is required to develop an approach for creating membranes with good mechanical stability while maintaining chain mobility. Thus, the low molecular weight PEG can be formed into a membrane by either (1) inducing chemical functionality to the high molecular weight polymer main chain or (2) physical mixing with the high molecular weight polymer.

In this study, we prepared poly(acrylic acid) (PAA/PEG) blend membranes with various PEG concentrations using an ethanol solvent to specifically target PEG-rich self-standing membranes. The high molecular weight PAA was used to provide the high mechanical strength while the low molecular weight PEG was used with a high weight loading to offer a strong CO<sub>2</sub> affinity to increase the solubility. The PAA/PEG blend membranes form a hydrogen bond between the carboxylate group of the PAA and the hydroxyl group of the PEG, which increases the physical stability and blending uniformity. As the PEG concentration is increased, the PAA/PEG blend membrane exhibits a lower glass transition temperature and higher surface hydrophilicity due to high mobility and rubbery characteristics. We evaluated CO<sub>2</sub> gas permeation properties such as CO<sub>2</sub> permeability and CO<sub>2</sub> selectivities over other gases (e.g., H<sub>2</sub>, N<sub>2</sub>, and CH<sub>4</sub>) for the PAA/PEG blend membranes. Additionally, the PAA/PEG blend membrane-based CO<sub>2</sub> separation performance was compared with other PEG-related membranes from the reported literature.

## 2. EXPERIMENTAL SECTION

**2.1. Materials.** PAA (poly(acrylic acid), average  $M_v \sim 4,000,000$  g/mol,  $M_v$  is the viscosity-average molecular weight), PEG (poly(ethylene glycol), average  $M_n \sim 400$  g/mol,  $M_n$  is the number average molecular weight), and PEGDE (poly(ethylene glycol)diglycidyl ether, average  $M_n \sim 500$  g/mol) were purchased from Sigma–Aldrich. Ethanol (EtOH, 94%) was purchased from Duxsan Chemicals. All commercial materials were used as received without any modification or purification.

**2.2. Membrane Fabrication.** The fabrication of the PAA/PEG blend membranes involved solution casting and solvent evaporation. The PAA/PEG blend solution concentration and PAA/PEG blend ratio were controlled to demonstrate the physicochemical properties of membranes with various PEG concentrations. For example, for PAA/PEG(1:9, 2:8, 3:7, and 4:6) blend membranes, PAA (0.05, 0.1, 0.099, and 0.132 g) was dissolved in EtOH solvent (all 12 mL) at room temperature. Subsequently, PEG (0.45, 0.4, 0.231, and 0.198 g) was added to each PAA polymer solution followed by stirring for 8 h to form a homogeneous PAA/PEG blend

solution. The prepared solution was poured onto a Teflon dish. The solvent was slowly evaporated in an oven at 60 °C for 24 h. The Teflon dish was covered with aluminum foil and treated with a few small holes to control the evaporation rate. The residual solvent was removed in a vacuum oven at 60 °C for 24 h after a complete drying process. It is noteworthy that the PAA/PEG(1:9 and 2:8) membranes were prepared with a solution concentration of 4 wt %, and the PAA/PEG(3:7 and 4:6) membranes were prepared with a solution concentration of 2.7 wt %. Based on these concentrations, we could obtain a uniform membrane when manufactured using a self-standing method. The resultant membrane had a thickness in the range of 100–150 μm. For the control experiment, a PAA/PEGDE(2:8) blend solution was prepared by dissolving PAA (0.1 g) and PEGDE (0.4 g) in EtOH solvent, and the membrane was formed using the same method. Moreover, the chemically cross-linked PEGDA membrane was obtained through the following experiments. PEGDA (0.45 g) and AIBN (0.05 g) were dissolved in ethanol solvent (4.5 mL), stirred, and then cast into a glass dish. The solvent was evaporated in an oven at 50 °C. After evaporating the solvent, the glass dish was transferred to an oven at 80 °C to proceed with cross-linking of PEGDA.

**2.3. Gas Permeation Test.** We tested the permeation of pure gases (H<sub>2</sub>, N<sub>2</sub>, CH<sub>4</sub>, and CO<sub>2</sub>) using a homemade pressure variable/volume constant system (Maxwell Robotics, USA). The gas transport properties of the membranes were measured using a time-lag method based on a solution–diffusion model. The fabricated membrane was attached to an impermeable brass disk using an epoxy adhesive (Devcon 5-minute epoxy). The membrane thickness was measured at least 5 times to calculate the membrane thickness, the active area of the membrane was calculated using a scanner and the ImageJ software program before performing the permeation test, and the coupon was loaded into the permeation cell and exposed to sufficiently dynamic vacuum conditions for at least 6 h. An air-heating circulator was used to maintain the temperature at 35 °C. Before the permeation test, a leak test was performed to determine the correct gas transfer rate. The upstream pressures were progressively set to 150 psi for the pure gases (H<sub>2</sub>, N<sub>2</sub>, CH<sub>4</sub>, and CO<sub>2</sub>), while the downstream pressure was set under static vacuum conditions. Permeation tests were performed for all gases until the gas transport rate reached a steady state.

Permeability and selectivity are two important parameters in the transport properties of membranes. Pure gas permeability is related to the rate of gas transport at which a gas species permeates through a membrane. The pure gas permeability is expressed as

$$P_i = \frac{Vl}{p_2 ART} \left[ \left( \frac{dp_i}{dt} \right)_{ss} - \left( \frac{dp_i}{dt} \right)_{leak} \right],$$

where  $V$  is the downstream volume (cm<sup>3</sup>),  $l$  is the membrane thickness (cm),  $p_2$  is the upstream pressure (cmHg),  $A$  is the active area of membrane (cm<sup>2</sup>),  $R$  is the ideal gas constant,  $T$  is the system temperature (K),  $\left( \frac{dp_i}{dt} \right)_{ss}$  is the rate of downstream pressure increase (cmHg/s), and  $\left( \frac{dp_i}{dt} \right)_{leak}$  is the leak rate (cmHg/s).

The ideal gas selectivity,  $(\alpha_{ij})$ , is the separation efficiency; the rate at which a particular gas of interest permeates the

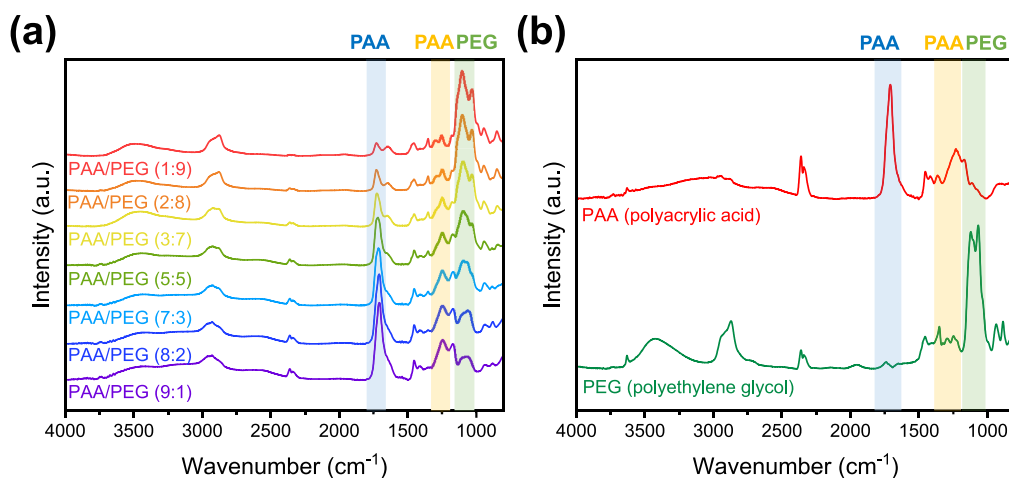


**Figure 1.** FT-IR spectra of (a) PAA/PEG blend with various PEG weight loadings and (b) pure PAA and pure PEG.

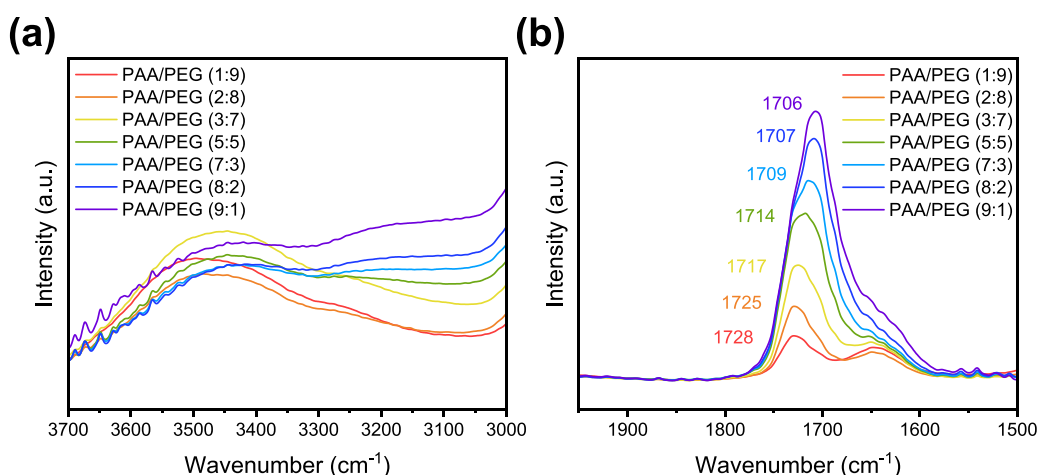


**Figure 2.** FT-IR spectra of the PAA/PEG blend membranes in the enlarged wavenumber range of (a) 3000–3700  $\text{cm}^{-1}$  for the hydroxyl group and (b) 1950–1500  $\text{cm}^{-1}$  for the carboxylate group.

membrane compared to other gas species. The ideal gas selectivity is expressed as

$$\alpha_{i/j} = P_i/P_j$$

**2.4. Characterization.** Fourier-transform infrared spectroscopy (FT-IR) analysis was conducted using an FT-IR instrument (Spectrum 100, PerkinElmer, USA). The FT-IR spectra were recorded from 500 to 4000  $\text{cm}^{-1}$  at a resolution of 4  $\text{cm}^{-1}$  with 16 scans. At the Chonnam National University Engineering Practical Education Center, thermogravimetric analysis (TGA) was performed using a thermogravimetric analyzer (TGA2, Mettler Toledo, Swiss) to determine the weight loss curve as a function of temperature under a  $\text{N}_2$  atmosphere from 30 to 800  $^{\circ}\text{C}$  with a scan rate of 10  $^{\circ}\text{C}/\text{min}$ . At the Chonnam National University Engineering Practical Education Center, differential scanning calorimetry (DSC) analysis was performed using a DSC instrument (DSC3, Mettler Toledo, Swiss) to determine the glass transition temperature ( $T_g$ ). The temperature was increased from  $-70$  to 150  $^{\circ}\text{C}$  at a heating rate of 10  $^{\circ}\text{C}/\text{min}$  under a  $\text{N}_2$  atmosphere, and the second sequential data was used to estimate the  $T_g$  value. The water contact angle was measured using a goniometer (Phoenix 300, SEO, South Korea) by dropping the water on the membrane surface. Optical microscope images were taken using an EG Tech EGVM-452M video

microscope system. The physical stability and water-absorbing ability under humid conditions were demonstrated in a temperature and humidity-controllable chamber (TH3-ME-025, JEIO TECH, South Korea).

### 3. RESULTS AND DISCUSSION

**3.1. Chemical Structure of PAA/PEG Blend Membranes.** Figure 1a presents the FT-IR spectrum of the PAA/PEG blend membranes with various PEG weight loadings. The FT-IR spectra of the PAA exhibited absorption bands at approximately 3550 and 3150  $\text{cm}^{-1}$ , corresponding to the free hydroxyl group and hydroxyl groups with hydrogen bonds.<sup>26</sup> In Figure 1b, the PEG shows the representative absorption bands at 1000–1200  $\text{cm}^{-1}$  that are attributable to the C–O–C stretching vibration mode. Further, the PAA exhibited noticeable peaks at 1700  $\text{cm}^{-1}$  due to the –COOH stretching vibration mode and a peak at 1246  $\text{cm}^{-1}$  due to combined C–O and O–H in-plane bending vibrations.<sup>27,28</sup> As the PEG weight loading in the PAA/PEG blend membrane was increased, the intensity of PEG characteristic peaks at 1104 and 1032  $\text{cm}^{-1}$  also increased (green-highlighted). However, the intensity of the PAA characteristic peaks at 1246  $\text{cm}^{-1}$  (yellow-highlighted) and 1700  $\text{cm}^{-1}$  (blue-highlighted) decreased. None of the PAA/PEG blend membranes exhibited

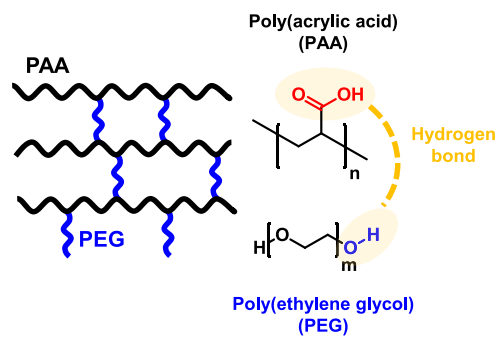
new absorption bands, indicating that the blend membrane was just physically mixed without any new chemical reaction.

Figure 2 shows the detailed FT-IR peak shift of the PAA/PEG blend membranes with various PEG weight loadings. A decrease in the peak intensity at  $3150\text{ cm}^{-1}$  was observed in the PAA/PEG blend membrane with a higher PEG weight loading (Figure 2a). This was because the intramolecular hydrogen bond between each carboxylate group of the PAA was transformed into a new intermolecular hydrogen bond between the hydroxyl group of the PEG and the carboxylate group of the PAA. The shifts of the free and bound hydroxyl bands indicate that the  $-\text{OH}$  groups in the blend are different from the PAA alone, and thus the shape of the hydroxyl bands indicates that free hydrogen bonds and intermolecular hydrogen bonds are present in the PAA/PEG mixture.<sup>26,29</sup>

We can further see the hydrogen bond between the PAA and PEG in the PAA/PEG blend membrane in Figure 2b. In the FT-IR spectra of the PAA/PEG blend membrane, the carbonyl stretching vibration mode can be seen with both the free carbonyl group and the inter-(or intra-)molecular hydrogen bond. The PAA/PEG(9:1) FT-IR spectra revealed an absorption band at  $1706\text{ cm}^{-1}$ . The absorption band at the corresponding wavenumber shifts to a higher wavenumber when the PAA/PEG blend membrane becomes the PEG-rich blend membrane. This is because the self-associated carboxylate group is converted to the intermolecular hydrogen bond formation between the carboxylate group of the PAA and the hydroxyl group of the PEG.<sup>30</sup> Thus, the distinctive peak of the carbonyl stretching vibration mode shifted from  $1706$  to  $1728\text{ cm}^{-1}$  as the PEG content in the PAA/PEG blend membrane increased from 9:1 to 1:9. The inter- and intramolecular interaction can contribute to forming macromolecular polymers with more complex chain structures (e.g., lattice structures).<sup>31,32</sup> Thus, the PAA/PEG blend membrane with the inter- and intramolecular interaction enabled the physically strong frame with the well-blended state.<sup>31,32</sup> The hydrogen bond between PAA and PEG also can be formed between the carboxylic acid group of PAA and the ether group of the PEG backbone.<sup>33–36</sup> To further demonstrate the hydrogen bonding effect between the hydroxyl end group of the PEG (not the ether group of the PEG backbone) and the carboxylic acid group of PAA, we formed the PAA/PEGDE (2:8) blend membrane with PEGDE, which does not have the hydroxyl end group. Figure S1 shows the FT-IR spectra of PAA, PAA/PEG(2:8), PAA/PEGDE(2:8), and PEGDE. Compared to the pristine PAA, the PAA/PEG(2:8) blend membrane showed a significant shift of the carbonyl stretching vibration mode peak to a higher wavenumber due to the strong hydrogen bond between the carboxylate group of the PAA and both hydroxyl and ether groups of the PEG as shown in Scheme 1. Meanwhile, the PAA/PEGDE(2:8) blend membrane exhibited a slight peak shift of the carbonyl stretching vibration mode attributable to the moderate hydrogen bond between the carboxylate group of the PAA and the ether group of the PEG. Thus, the hydrogen bond between the carboxylate group of the PAA and the ether group of the PEG occurred but the hydrogen bond between the carboxylate group of the PAA and the hydroxyl group of the PEG also happened.

**3.2. Thermal Properties of PAA/PEG Blend Membranes.** We demonstrated the thermal stability and  $T_g$  of the PAA/PEG blend membranes with various PEG concentrations (PAA/PEG = 4:6, 3:7, 2:8, and 1:9). Figure 3a shows the weight loss curve of the PAA/PEG blend membranes as a

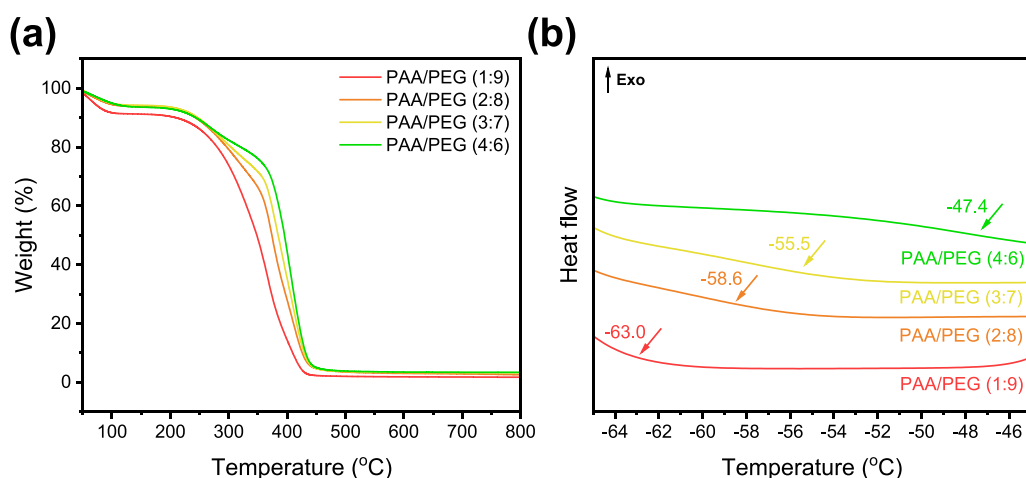
**Scheme 1. PAA/PEG Blend Membrane with Hydrogen Bonds**



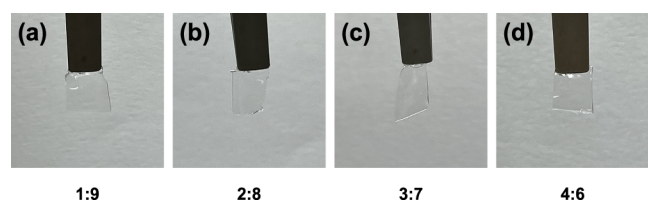
function of temperature in a  $\text{N}_2$  atmosphere. For the PAA/PEG blend membranes, the TGA profile can be divided into three distinguishable steps. The initial weight loss occurred at approximately  $50\text{--}100\text{ }^\circ\text{C}$  due to residual solvent (e.g., ethanol and water molecules), which resulted from the membrane fabrication process and moisture in the ambient conditions even after the complete drying process. Although we completely dried the PAA/PEG blend membrane in a vacuum oven, the PAA and PEG phases still contained slight ethanol solvent and water molecules owing to their high hydrophilicity. The second weight loss step occurred between  $200$  and  $300\text{ }^\circ\text{C}$ . This was due to the partial decomposition of the PEG and the carboxylate dehydration of the PAA.<sup>19,37,38</sup> The third weight loss step occurred above  $300\text{ }^\circ\text{C}$  owing to the main polymer chain structural decomposition of the PAA and PEG.<sup>39</sup> Particularly, the high PAA loading-based PAA/PEG blend membrane exhibited higher thermal stability at about  $400\text{ }^\circ\text{C}$  than the PEG-rich PAA/PEG blend membrane. This phenomenon was probably due to the high thermal stability of the PAA polymer as well as the high molecular weight and hydrocarbon-based main chain. In contrast, the PEG has a relatively lower molecular weight and low temperature-resistant ether bond in its main chain.

Figure 3b shows the second sequential DSC curve of the PAA/PEG blend membranes for  $T_g$  assessment. The enlarged and separate DSC curves of the PAA/PEG blend membranes are shown in Figure S2 to determine the  $T_g$  with a noticeable inflection point. For the precise  $T_g$  demonstration, the PAA/PEG blend membranes were fully dried in a vacuum oven to completely remove the absorbed moisture before running the DSC scan. The  $T_g$  was estimated from a second heating sequential curve.<sup>40</sup> The PAA/PEG(3:7 and 2:8) blend membranes with high PEG weight loadings exhibited amorphous properties with PAA-PEG hydrogen bonding interactions, resulting in a single  $T_g$  associated with PEG in Figure S3a.<sup>30</sup> However, the PAA/PEG(4:6) mixed membrane exhibited a slight transition at  $119\text{ }^\circ\text{C}$  due to the relatively high PAA content and possessed two  $T_g$ s (Figure S3b). It can be seen that this is similar to the typical  $T_g$  values of PAA (above  $110\text{ }^\circ\text{C}$ ) specified in the literature.<sup>41,42</sup> Meanwhile, the low  $T_g$  of the PAA/PEG blend membranes (PAA/PEG = 4:6, 3:7, 2:8, and 1:9) was shown at from  $-40$  to  $-60\text{ }^\circ\text{C}$  due to the rubbery PEG. As the PEG content in the PAA/PEG blend membrane increased, the  $T_g$  further decreased from  $-47.4$  to  $-63\text{ }^\circ\text{C}$ .<sup>43,44</sup>

**3.3. Morphological and Surface Properties of PAA/PEG Blend Membranes.** Figure 4 presents photographs of the self-standing PAA/PEG blend membranes. All the membranes were homogeneous, transparent, and flexible



**Figure 3.** (a) TGA profile and (b) DSC curve of the PAA/PEG blend membranes with various PEG concentrations (PAA/PEG = 1:9, 2:8, 3:7, and 4:6).



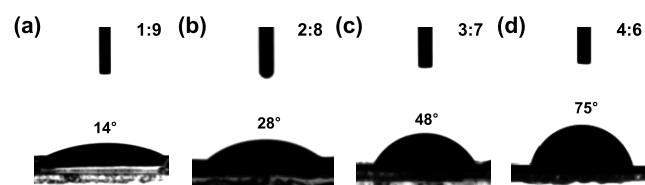
**Figure 4.** Photographs of the PAA/PEG blend membranes with various PEG concentrations (PAA/PEG = (a) 1:9, (b) 2:8, (c) 3:7, and (d) 4:6).

with proper mechanical properties owing to the high PAA molecular weight, even with high PEG weight loading. Moreover, Figure S4 shows the optical microscope images of PAA/PEG blend membranes with various PEG weight loadings. The PAA/PEG blend membranes exhibited uniform and defect-free surface morphology, which indicates the well-blended state of the PAA and PEG in the membrane. Particularly, the PAA/PEG blend membrane with a high PEG weight loading was slightly sticky because of the rubbery nature of the PEG content.

Thus, we were not able to perform the UTM (universal testing machine) test to demonstrate the mechanical properties of the PAA/PEG blend membranes. Instead of performing the UTM test, we took a few photos to demonstrate the mechanical characteristics of PAA/PEG blend membranes, mainly exhibiting the potential as a suitable adhesive by preventing membrane deformation even with a high gravity force. Figure S5 shows the PAA/PEG(3:7) blend membrane attached to a few objects (glass vial, slide glass, glass dish). Even under additional gravity force, the small area of the PAA/PEG(3:7) blend membrane maintained its shape without being torn out. This result indicates that the PAA/PEG blend membrane with the low molecular PEG has a high mechanical strength that can withstand the heavy weight of the object. We further fabricated a chemically cross-linked PEGDA membrane to compare with the PAA/PEG blend membrane. Figure S6 shows the photograph and FT-IR spectra of the cross-linked PEGDA membrane. The cross-linked PEGDA membrane was visually transparent and uniform but it was difficult to stretch and break because of the high hardness in Figure S6a. This is consistent with the low absorption band at approximately 3400 cm<sup>-1</sup> attributable to the relatively less absorbed water

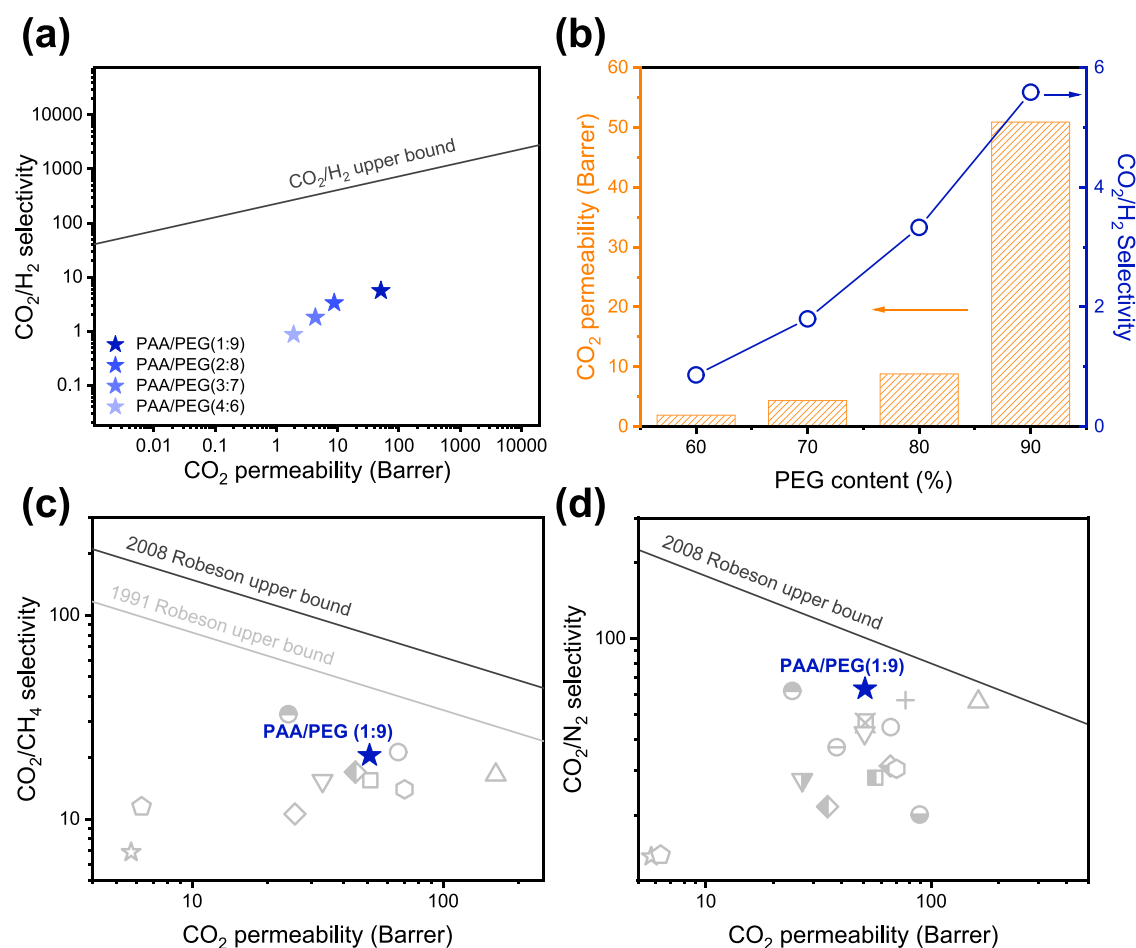
molecules in the cross-linked PEGDA membrane. On the other hand, the PEG/PAA blend membrane was sticky and stretchy due to the free PEG-rich domain. In addition, the PEG/PAA blend membrane included more water molecules compared to the cross-linked PEGDA membrane as shown in Figure S6b. Of practical importance, the PAA/PEG blend membrane has manufacturing advantages such as easy-to-tune PEG concentration and a simple fabrication method.

Figure 5 depicts the water contact angle values of the PAA/PEG blend membranes with various PEG weight loadings. The



**Figure 5.** Water contact angle of the PAA/PEG blend membranes with various PEG concentrations (PAA/PEG = (a) 1:9, (b) 2:8, (c) 3:7, and (d) 4:6).

PAA/PEG blend membrane with higher PEG concentrations had a hydrophilic surface. Thus, the water contact angle value was lower when a more PEG-rich PAA/PEG blend membrane was formed. The PAA/PEG(4:6) blend membrane had a water contact angle value of 75° while the PAA/PEG(1:9) blend membrane had a water contact angle value of 14°. This result indicates the presence of high PEG weight loading in the homogeneous PAA/PEG blend membrane.<sup>45</sup> In addition, we tracked the physical stability and performed FT-IR analysis after placing the membrane sample under various relative humidities using a temperature and humidity-controllable chamber to confirm that the PAA/PEG blend membrane is mechanically stable under high-humidity environments. The PAA/PEG(3:7) blend membrane was placed in the temperature and humidity-controllable chamber for 12 h under 30%, 60%, and 90% RH. The PAA/PEG(3:7) blend membrane did not show mechanical differences, maintaining the same external morphology and area. Meanwhile, the PAA/PEG(3:7) blend membrane showed an enhanced peak intensity at approximately 3400 cm<sup>-1</sup> due to absorbed water molecules in the PAA/PEG(3:7) blend membrane under humid conditions as shown in Figure S7. Thus, this result



**Figure 6.** CO<sub>2</sub> separation performance of the PAA/PEG blend membranes with various PEG concentrations (PAA/PEG = 1:9, 2:8, 3:7, and 4:6) at 35 °C and 150 psi: (a) CO<sub>2</sub>/H<sub>2</sub> separation performance with the upper bound limit, (b) CO<sub>2</sub> permeability and CO<sub>2</sub>/H<sub>2</sub> selectivity as a function of PEG contents. (c) CO<sub>2</sub>/CH<sub>4</sub> separation performance of the PAA/PEG(1:9) blend membranes at 35 °C and 150 psi with PEG-related reported literature data (star, closed: PAA/PEG(1:9), box, open: Pebax/PEG 200 (50 wt %), star, open: CA + 10% PEG 600, pentagon: CA + 10% PEG 2000, upright triangle: P-PEGDME (10), circle, open: P-PEG10000 (10), circle, upper shaded: HDI-BDO/PEG2000, hexagon: PVC-g-POEM, inverted triangle: Matrimid-PEG+30 wt % ZIF-8, diamond: PEBAX-1074/PEG-1500, diamond, left shaded: MDI-DAE/PEG1500) and the Robeson upper bound limits, and (d) CO<sub>2</sub>/N<sub>2</sub> separation performance of the PAA/PEG (1:9) blend membranes at 35 °C and 150 psi with PEG-related reported literature data (star, closed: PAA/PEG(1:9), box, open: Pebax/PEG 200 (50 wt %), star, open: CA + 10% PEG 600, pentagon: CA + 10% PEG 2000, upright triangle: P-PEGDME (10), circle, open: P-PEG10000 (10), circle, upper shaded: HDI-BDO/PEG2000, hexagon: PVC-g-POEM, inverted triangle, right shaded: PES-g-PEG, diamond, left shaded: PVA-g-POEM, cross: PGMA-co-POEM, circle, target: PVBC-BITFSI(5%)/BMIMTFSI, inverted triangle: PCZ-r-PEG 2000 (H), diamond, bottom shaded: Silane Cross-linked PEG 2000(2:1), box, left shaded: BI-PEG4-Xpi, plus: Thiol-containing PEG, circle, bottom shaded: PVA/PEG 600(40 wt %)) and the Robeson upper bound limits.

indicates that the PAA/PEG(3:7) blend membrane was physically stable under high RH conditions. In addition, the PAA/PEG(3:7) blend membrane effectively absorbed the water molecules, which can be potentially employed for gas separation under wet conditions.

**3.4. Gas Permeation Properties of PAA/PEG Blend Membranes.** Figure 6 shows the CO<sub>2</sub> gas separation performance of the PAA/PEG blend membranes with various PEG concentrations measured at 35 °C and 150 psi. Figure 6a and Table 1 show the CO<sub>2</sub> permeability and CO<sub>2</sub>/H<sub>2</sub> selectivity of the PAA/PEG blend membranes as a function of PEG weight loading. The CO<sub>2</sub> permeability and CO<sub>2</sub>/H<sub>2</sub> selectivity of the PAA/PEG blend membrane proportionally increased as the PEG concentration increased, until reaching the upper bound limit. This was due to the ethylene oxide (EO) unit of the PEG, which has a polar ether portion and can exhibit a high CO<sub>2</sub> affinity.<sup>11</sup> Thus, the PEG with the EO unit can interact with CO<sub>2</sub> molecules by quadruple interaction. As a

**Table 1.** H<sub>2</sub> and CO<sub>2</sub> Permeation Properties of the PAA/PEG Blend Membranes with Various PEG Concentrations at 35 °C and 150 psi

	$P(\text{H}_2)$ (Barrer)	$P(\text{CO}_2)$ (Barrer)	CO <sub>2</sub> /H <sub>2</sub>
PAA/PEG(1:9)	9.1	50.9	5.6
PAA/PEG(2:8)	2.6	8.8	3.3
PAA/PEG(3:7)	2.4	4.3	1.8
PAA/PEG(4:6)	2.2	1.9	0.9

result, the PAA/PEG blend membrane with a high PEG weight loading showed an improved CO<sub>2</sub> permeability. Additionally, for the PAA/PEG membranes, we chose the low molecular weight PEG instead of the high average molar mass PEO. The high average molar mass PEO is traditionally crystalline; hence, it cannot provide gas molecule-selective properties. Meanwhile, the low molecular weight PEG offers the mobile polymer chain and, as a result, CO<sub>2</sub>-selective characteristics based on the quadruple interaction. Table 2 shows that the PAA/PEG(1:9)

**Table 2. H<sub>2</sub>, N<sub>2</sub>, CH<sub>4</sub>, and CO<sub>2</sub> Permeation Properties of PAA/PEG(1:9) Blend Membrane at 35 °C and 150 psi**

sample	<i>P</i> (H <sub>2</sub> ) (Barrer)	<i>P</i> (N <sub>2</sub> ) (Barrer)	<i>P</i> (CH <sub>4</sub> ) (Barrer)	<i>P</i> (CO <sub>2</sub> ) (Barrer)	CO <sub>2</sub> /N <sub>2</sub>	CO <sub>2</sub> /CH <sub>4</sub>	CO <sub>2</sub> /H <sub>2</sub>	H <sub>2</sub> /N <sub>2</sub>	H <sub>2</sub> /CH <sub>4</sub>
PAA/PEG(1:9)	9.1	0.8	2.5	50.9	63.2	20.5	5.6	11.3	3.7

**Table 3. CO<sub>2</sub>/CH<sub>4</sub> Gas Separation Performance of the PAA/PEG(1:9) Blend Membrane with the Comparison of PEG-Related Reported Literature Data<sup>a</sup>**

sample	<i>P</i> (CO <sub>2</sub> )	<i>P</i> (CH <sub>4</sub> )	<i>P</i> (N <sub>2</sub> )	<i>P</i> (CO <sub>2</sub> )/ <i>P</i> (CH <sub>4</sub> )	<i>P</i> (CO <sub>2</sub> )/ <i>P</i> (N <sub>2</sub> )	reference
PAA-PEG(1:9)	50.9	2.5	0.8	20.5	63.2	this work
Pebax/PEG 200 (50 wt %)	51.3	3.3	1.1	15.5	47	10
CA + 10% PEG 600	5.7	0.831	0.418	6.88	13.7	46
CA + 10% PEG 2000	6.3	0.549	0.452	11.5	13.9	
P-PEGDME (10)	162	9.81	2.881	16.5	56.22	43
P-PEG10000 (10)	66.2	3.107	1.484	21.3	44.6	
HDI-BDO/PEG2000	24.2	0.74	0.39	32.7	62	47
PVC-g-POEM	70.2	5.0	2.3	14.0	30.5	21
Matrimid-PEG + 30 wt % ZIF-8	33.1	2.15		15.4		11
PEBAX-1074/PEG-1500	25.7	2.42		10.6		48,49
MDI-DAE/PEG1500	44.7	2.7		17		50
PES-g-PEG	26.8		0.97		27.6	51
PVA-g-POEM	34.7		1.6		21.6	52
PGMA-co-POEM	51		1.1		46.3	53
PVBC-BITFSI(5%)/BMIMTFSI	38.1		1.02		37.1	54
PCZ- <i>r</i> -PEG 2000 (H)	50.7		1.2		42.25	55
silane cross-linked PEG 2000(2:1)	66		2.1		31.3	44
BI-PEG4-xPI	56.52		2.01		28.12	56
thiol-containing PEG	77		1.35		57	23,57
PVA/PEG 600(40 wt %)	89		4.4		20.1	19

<sup>a</sup>(star, closed: PAA/PEG(1:9), box, open: Pebax/PEG 200 (50 wt %), star, open: CA + 10% PEG 600, pentagon: CA + 10% PEG 2000, upright triangle: P-PEGDME (10), circle, open: P-PEG10000 (10), circle, upper shaded: HDI-BDO/PEG2000, hexagon: PVC-g-POEM, inverted triangle: Matrimid-PEG+30 wt % ZIF-8, diamond: PEBAX-1074/PEG-1500, diamond, left shaded: MDI-DAE/PEG1500) and CO<sub>2</sub>/N<sub>2</sub> (star, closed: PAA/PEG(1:9), box, open: Pebax/PEG 200 (50 wt %), star, open: CA + 10% PEG 600, pentagon: CA + 10% PEG 2000, upright triangle: P-PEGDME (10), circle, open: P-PEG10000 (10), circle, upper shaded: HDI-BDO/PEG2000, hexagon: PVC-g-POEM, inverted triangle, right shaded: PES-g-PEG, diamond, left shaded: PVA-g-POEM, cross: PGMA-co-POEM, circle, target: PVBC-BITFSI(5%)/BMIMTFSI, inverted triangle: PCZ-*r*-PEG 2000 (H), diamond, bottom shaded: silane cross-linked PEG 2000(2:1), box, left shaded: BI-PEG4-Xpi, plus: thiol-containing PEG, circle, bottom shaded: PVA/PEG 600(40 wt %)).

blend membrane has the greatest potential for CO<sub>2</sub> separation when compared to other gas species (e.g., N<sub>2</sub> and CH<sub>4</sub>). The PAA/PEG(1:9) blend membrane shows a CO<sub>2</sub> permeability of 51 Barrer, with CO<sub>2</sub>/N<sub>2</sub> and CO<sub>2</sub>/CH<sub>4</sub> selectivities of 63 and 21, respectively. It should be noted that while other PAA/PEG blend membranes (2:8, 3:7, and 4:6) showed measurable H<sub>2</sub> and CO<sub>2</sub> permeabilities, N<sub>2</sub> and CH<sub>4</sub> permeabilities were significantly low. Therefore, we did not report the CO<sub>2</sub>/N<sub>2</sub> and CO<sub>2</sub>/CH<sub>4</sub> separation properties of the PAA/PEG blend membranes (2:8, 3:7, and 4:6) in this work. Figure 6c,d shows the CO<sub>2</sub>/CH<sub>4</sub> and CO<sub>2</sub>/N<sub>2</sub> separation performance of the PAA/PEG(1:9) blend membrane with other PEG-related membranes from the previously reported literature. We can see that the PAA/PEG(1:9) blend membrane exhibited a moderate CO<sub>2</sub> permeability with a high level of CO<sub>2</sub>/CH<sub>4</sub> and CO<sub>2</sub>/N<sub>2</sub> selectivities compared to other literature data (Table 3). Although our work on the PAA/PEG(1:9) blend membrane did not exceed the 1991 Robeson upper bound limit, this facile strategy provides good insight into fabricating PEG-rich self-standing membranes based on the simple fabrication method, good processability, and cost-effectiveness for efficient CO<sub>2</sub> separation.

#### 4. CONCLUSIONS

We report a self-standing PAA/PEG blend membrane with a high PEG weight loading using an ethanol solvent-based

solution casting method for CO<sub>2</sub> separation. Owing to the high molecular weight of PAA, the PAA/PEG blend membrane with a high PEG weight loading can be formed with the necessary mechanical properties. The PAA/PEG blend membrane shows the hydrogen bonds between (1) each carbonyl group of the PAA (or hydroxyl group of the PEG) and (2) the carbonyl group of the PAA as well as the hydroxyl group of the PEG. The increased temperature-dependent weight loss and decreased glass transition temperature of the PAA/PEG blend membranes indicate a proportional increase in PEG content during the homogeneous polymer blending. A similar trend was observed from the water contact angle value of the PAA/PEG, showing that the PEG-rich blend membrane exhibited further hydrophilicity in membrane surface characteristics. The PAA/PEG(1:9) blend membrane, which has the highest PEG concentration, exhibited an appropriate CO<sub>2</sub> permeability of 51 Barrer with high CO<sub>2</sub>/N<sub>2</sub> and CO<sub>2</sub>/CH<sub>4</sub> selectivities of 63 and 21, respectively. The high CO<sub>2</sub> affinity and chain mobility of EO units in the low molecular weight PEG contributed to the increase in CO<sub>2</sub> separation performance while maintaining the membrane conformation. This was due to the high molecular weight PAA even with the high PEG weight loading. This PEG-rich blend membrane strategy provides a good insight into forming alcohol solvent-induced simple membranes with good processability and cost-effectiveness for prospective CO<sub>2</sub> separation.

## ■ ASSOCIATED CONTENT

### SI Supporting Information

The Supporting Information is available free of charge at <https://pubs.acs.org/doi/10.1021/acsomega.2c06143>.

FT-IR data for comparison with pure PEGDE, additional data on DSC, optical microscopy images, photographs showing mechanical properties, FT-IR data for comparison with cross-linked PEGDA, and FT-IR data under various humidity conditions (PDF)

## ■ AUTHOR INFORMATION

### Corresponding Authors

**Jae Hun Lee** – Hydrogen Research Department, Korea Institute of Energy Research, Daejeon 34129, Republic of Korea; Email: [jhlee@kier.re.kr](mailto:jhlee@kier.re.kr)

**Won Seok Chi** – Department of Polymer Engineering, Graduate School and School of Polymer Science and Engineering, Chonnam National University, Gwangju 61186, Republic of Korea; [orcid.org/0000-0002-0422-0495](https://orcid.org/0000-0002-0422-0495); Email: [wschi@jnu.ac.kr](mailto:wschi@jnu.ac.kr)

### Authors

**Somi Yu** – Department of Polymer Engineering, Graduate School, Chonnam National University, Gwangju 61186, Republic of Korea

**Seong Jin An** – Department of Polymer Engineering, Graduate School, Chonnam National University, Gwangju 61186, Republic of Korea

**Ki Jung Kim** – Department of Polymer Engineering, Graduate School, Chonnam National University, Gwangju 61186, Republic of Korea

Complete contact information is available at:

<https://pubs.acs.org/10.1021/acsomega.2c06143>

### Notes

The authors declare no competing financial interest.

## ■ ACKNOWLEDGMENTS

This work was supported by the National Research Foundation of Korea (NRF) and grant-funded by the Korean government (MSIP) (NRF-2020R1F1A1075098), Nano-Material Technology Development Program through the National Research Foundation of Korea (NRF) funded by the Ministry of Science, ICT and Future Planning (2009-0082580), the Korea Institute of Energy Technology Evaluation and Planning (KETEP), and the Ministry of Trade, Industry & Energy (MOTIE) of the Republic of Korea (No. 20218520040040).

## ■ REFERENCES

- (1) Wang, S.; Li, X.; Wu, H.; Tian, Z.; Xin, Q.; He, G.; Peng, D.; Chen, S.; Yin, Y.; Jiang, Z.; Guiver, M. D. Advances in High Permeability Polymer-Based Membrane Materials for CO<sub>2</sub> Separations. *Energy Environ. Sci.* **2016**, *9*, 1863.
- (2) Du, N.; Park, H. B.; Dal-Cin, M. M.; Guiver, M. D. Advances in High Permeability Polymeric Membrane Materials for CO<sub>2</sub> Separations. *2012*, *5* (6), 7306–7322, DOI: [10.1039/c1ee02668b](https://doi.org/10.1039/c1ee02668b).
- (3) Powell, C. E.; Qiao, G. G. Polymeric CO<sub>2</sub>/N<sub>2</sub> Gas Separation Membranes for the Capture of Carbon Dioxide from Power Plant Flue Gases. *J. Membr. Sci.* **2006**, *279*, 1–49.
- (4) Han, Y.; Yang, Y.; Ho, W. S. W. Membranes Recent Progress in the Engineering of Polymeric Membranes for CO<sub>2</sub> Capture from Flue Gas. *2020*, *10* (11), 365, DOI: [10.3390/membranes10110365](https://doi.org/10.3390/membranes10110365).
- (5) Han, Y.; Ho, W. S. W. Polymeric Membranes for CO<sub>2</sub> Separation and Capture. *J. Membr. Sci.* **2021**, *628*, No. 119244.
- (6) Baker, R. W.; Lokhandwala, K. Natural Gas Processing with Membranes: An Overview. *Ind. Eng. Chem. Res.* **2008**, *47*, 2109.
- (7) Ghadimi, A.; Amirilargani, M.; Mohammadi, T.; Kasiri, N.; Sadatnia, B. Preparation of Alloyed Poly(Ether Block Amide)/Poly(Ethylene Glycol Diacrylate) Membranes for Separation of CO<sub>2</sub>/H<sub>2</sub> (Syngas Application). *J. Membr. Sci.* **2014**, *458*, 14–26.
- (8) Voldsund, M.; Jordal, K.; Anantharaman, R. Hydrogen Production with CO<sub>2</sub> Capture. *Int. J. Hydrogen Energy* **2016**, *41*, 4969–4992.
- (9) Lin, H.; Freeman, B. D. Materials Selection Guidelines for Membranes That Remove CO<sub>2</sub> from Gas Mixtures. *J. Mol. Struct.* **2005**, *739*, 57–74.
- (10) Car, A.; Stropnik, C.; Yave, W.; Peinemann, K. V. PEG Modified Poly(Amide-b-Ethylene Oxide) Membranes for CO<sub>2</sub> Separation. *J. Membr. Sci.* **2008**, *307*, 88–95.
- (11) Castro-Muñoz, R.; Fila, V.; Martin-Gil, V.; Muller, C. Enhanced CO<sub>2</sub> Permeability in Matrimid 5218 Mixed Matrix Membranes for Separating Binary CO<sub>2</sub>/CH<sub>4</sub> Mixtures. *Sep. Purif. Technol.* **2019**, *210*, 553–562.
- (12) Sholl, D. S.; Lively, R. P. Seven chemical separations to change the world. *Nature* **2016**, *532*, 435–437.
- (13) Baker, R. W.; Low, B. T. Gas Separation Membrane Materials: A Perspective. *2014*, *47*, 6999–7013, DOI: [10.1021/ma501488s](https://doi.org/10.1021/ma501488s).
- (14) Galizia, M.; Chi, W. S.; Smith, Z. P.; Merkel, T. C.; Baker, R. W.; Freeman, B. D. 50th Anniversary Perspective: Polymers and Mixed Matrix Membranes for Gas and Vapor Separation: A Review and Prospective Opportunities. *2017*, *50*, 7809–7843, DOI: [10.1021/acs.macromol.7b01718](https://doi.org/10.1021/acs.macromol.7b01718).
- (15) Qian, Q.; Asinger, P. A.; Lee, M. J.; Han, G.; Rodriguez, K. M.; Lin, S.; Benedetti, F. M.; Wu, A. X.; Chi, S.; Smith, Z. P. MOF-Based Membranes for Gas Separations. *2020*, *120*, 8161–8266, DOI: [10.1021/acs.chemrev.0c00119](https://doi.org/10.1021/acs.chemrev.0c00119).
- (16) Robeson, L. M. The Upper Bound Revisited. *J. Membr. Sci.* **2008**, *320*, 390–400.
- (17) Robeson, L. M. Correlation of Separation Factor versus Permeability for Polymeric Membranes. *J. Membr. Sci.* **1991**, *62*, 165–185.
- (18) Rowe, B. W.; Robeson, L. M.; Freeman, B. D.; Paul, D. R. Influence of Temperature on the Upper Bound: Theoretical Considerations and Comparison with Experimental Results. *J. Membr. Sci.* **2010**, *360*, 58–69.
- (19) Dilshad, M. R.; Islam, A.; Sabir, A.; Shafiq, M.; Butt, M. T. Z.; Ijaz, A.; Jamil, T. Fabrication and Performance Characterization of Novel Zinc Oxide Filled Cross-Linked PVA/PEG 600 Blended Membranes for CO<sub>2</sub>/N<sub>2</sub> Separation. *J. Ind. Eng. Chem.* **2017**, *55*, 65–73.
- (20) Lillepär, J.; Georgopoulos, P.; Shishatskiy, S. Stability of Blended Polymeric Materials for CO<sub>2</sub> Separation. *J. Membr. Sci.* **2014**, *467*, 269–278.
- (21) Chi, W. S.; Kim, S. J.; Lee, S. J.; Bae, Y. S.; Kim, J. H. Enhanced Performance of Mixed-Matrix Membranes through a Graft Copolymer-Directed Interface and Interaction Tuning Approach. *ChemSusChem* **2015**, *8*, 650–658.
- (22) Shin, H.; Chi, W. S.; Bae, S.; Kim, J. H.; Kim, J. High-Performance Thin PVC-POEM/ZIF-8 Mixed Matrix Membranes on Alumina Supports for CO<sub>2</sub>/CH<sub>4</sub> Separation. *J. Ind. Eng. Chem.* **2017**, *53*, 127–133.
- (23) Deng, J.; Dai, Z.; Yan, J.; Sandru, M.; Sandru, E.; Spontak, R. J.; Deng, L. Facile and Solvent-Free Fabrication of PEG-Based Membranes with Interpenetrating Networks for CO<sub>2</sub> Separation. *J. Membr. Sci.* **2019**, *570–571*, 455–463.
- (24) Kim, N. U.; Park, B. J.; Guiver, M. D.; Kim, J. H. Use of Non-Selective, High-Molecular-Weight Poly(Ethylene Oxide) Membrane for CO<sub>2</sub> Separation by Incorporation of Comb Copolymer. *J. Membr. Sci.* **2020**, *605*, No. 118092.
- (25) Lee, J. H.; Lim, J. Y.; Park, M. S.; Kim, J. H. Improvement in the CO<sub>2</sub> Permeation Properties of High-Molecular-Weight Poly(Ethylene

- Oxide): Use of Amine-Branched Poly(Amidoamine) Dendrimer. *2018*, *51* (21), 8800–8807, DOI: [10.1021/acs.macromol.8b02037](https://doi.org/10.1021/acs.macromol.8b02037).
- (26) De Chimie, R. R.; Ilie, C.; Stingă, G.; Iovescu, A.; Purcar, V.; Anghel, F. The Influence of Nonionic Surfactants on the Carbopol-Peg Interpolymer Complexes. *Rev. Roum. Chim.* **2010**, *55*, 409–417.
- (27) Madami, W.; Seoudi, R. Molecular and Fluorescence Spectroscopic Studies of Polyacrylic Acid Blended with Rhodamine B Mixed Gold Nanoparticles. *J. Taibah Univ. Sci.* **2020**, *14*, 790–799.
- (28) Cukrowicz, S.; Sitarz, M.; Kornaus, K.; Kaczmarek, K.; Bobrowski, A.; Gubernat, A.; Grabowska, B. Materials Organobentonites Modified with Poly(Acrylic Acid) and Its Sodium Salt for Foundry Applications. *2021*, *14*, 1947, DOI: [10.3390/ma14081947](https://doi.org/10.3390/ma14081947).
- (29) Alkan, C.; Günther, E.; Hiebler, S.; Himpel, M. Complexing Blends of Polyacrylic Acid-Polyethylene Glycol and Poly(Ethylene-Co-Acrylic Acid)-Polyethylene Glycol as Shape Stabilized Phase Change Materials. *Energy Convers. Manage.* **2012**, *64*, 364–370.
- (30) Liu, W. C.; Chung, C. H.; Hong, J. L. Highly Stretchable, Self-Healable Elastomers from Hydrogen-Bonded Interpolymer Complex (HIPC) and Their Use as Sensitive, Stable Electric Skin. *ACS Omega* **2018**, *3*, 11368–11382.
- (31) Jin, J.; Zheng, R. Q.; Zhou, Y. N.; Luo, Z. H. Network Formation Kinetics of Poly(Dimethylsiloxane) Based on Step-Growth Polymerization. *Macromolecules* **2021**, *54*, 7678–7689.
- (32) De Keer, L.; Kilic, K. I.; Van Steenberge, P. H. M.; Daelemans, L.; Kodura, D.; Frisch, H.; De Clerck, K.; Reyniers, M. F.; Barner-Kowollik, C.; Dauskardt, R. H.; D'hooge, D. R. Computational Prediction of the Molecular Configuration of Three-Dimensional Network Polymers. *Nat. Mater.* **2021**, *20*, 1422–1430.
- (33) Yu, X.; Tanaka, A.; Tanaka, K.; Tanaka, T. Phase Transition of a Poly (Acrylic Acid) Gel Induced by Polymer Complexation. *J. Chem. Phys.* **1992**, *97*, 7805–7808.
- (34) Lu, X.; Weiss, R. A. Phase Behavior of Blends of Poly(Ethylene Glycol) and Partially Neutralized Poly(Acrylic Acid). *Macromolecules* **1995**, *28*, 3022–3029.
- (35) Bailey, F. E.; Lukdberg, R. D.; Callard, R. W. Some Factors Meeting the Molecular Association of Poly(Ethylene Oxide) and Poly (Acrylic Acid) In Aqueous Solution\*. *J. Polym. Sci., Part A: Gen. Pap.* **1964**, *2*, 845–851.
- (36) Hao, J.; Yuan, G.; He, W.; Cheng, H.; Han, C. C.; Wu, C. Interchain Hydrogen-Bonding-Induced Association of Poly(Acrylic Acid)-Graft-Poly(Ethylene Oxide) in Water. *Macromolecules* **2010**, *43*, 2002–2008.
- (37) Khairuddin; Pramono, E.; Utomo, S. B.; Wulandari, V.; Zahrotul, A. W.; Clegg, F. The Effect of Polyethylene Glycol Mw 400 and 600 on Stability of Shellac Waxfree. *J. Phys.: Conf. Ser.* **2016**, *776*, No. 012054.
- (38) Sadeghpour, M.; Yusoff, R.; Aroua, M. K. Modification of Polyethylene Glycol with Choline Chloride and Evaluation of the CO<sub>2</sub> Absorption Capacity of Their Aqueous Solutions. *Science and Technology* **2018**, *8*, 324–334.
- (39) Ebadi, S. V.; Fakhrali, A.; Ranaei-Siadat, S. O.; Gharehaghaji, A. A.; Mazinani, S.; Dinari, M.; Harati, J. Immobilization of Acetylcholinesterase on Electrospun Poly(Acrylic Acid)/Multi-Walled Carbon Nanotube Nanofibrous Membranes. *RSC Adv.* **2015**, *5*, 42572–42579.
- (40) Vrandečić, N. S.; Erceg, M.; Jakić, M.; Klarić, I. Kinetic Analysis of Thermal Degradation of Poly(Ethylene Glycol) and Poly(Ethylene Oxide)s of Different Molecular Weight. *Thermochim. Acta* **2010**, *498*, 71–80.
- (41) Sofyan Sulaeman, A.; Adi Putro, P.; Nikmatin, S. Thermal Studies of Hydrogels Based on Poly(Acrylic Acid) and Its Copolymers by Differential Scanning Calorimetry: A Systematic Literature Review. *Polym. Polym. Compos.* **2022**, *30*, 1–10.
- (42) Wang, X.; Yang, Y.; Zhou, Y.; Wu, P.; Chen, H.; Trefonas, P. Hydrogen Bond Mediated Partially Miscible Poly(N-Acryloyl Piperidine)/Poly(Acrylic Acid) Blend with One Glass Transition Temperature. *Polymer* **2018**, *151*, 269–278.
- (43) Wang, S.; Liu, Y.; Huang, S.; Wu, H.; Li, Y.; Tian, Z.; Jiang, Z. Pebax-PEG-MWCNT Hybrid Membranes with Enhanced CO<sub>2</sub> Capture Properties. *J. Membr. Sci.* **2014**, *460*, 62–70.
- (44) Cong, H.; Yu, B. Aminosilane Cross-Linked PEG/PEPEG/PPEPG Membranes for CO<sub>2</sub>/N<sub>2</sub> and CO<sub>2</sub>/H<sub>2</sub> Separation. *2010*, *49* (19), 9363–9369, DOI: [10.1021/ie1012568](https://doi.org/10.1021/ie1012568).
- (45) Liu, L.; Gao, Y.; Zhao, J.; Yuan, L.; Li, C.; Liu, Z.; Hou, Z. A Mild Method for Surface-Grafting PEG Onto Segmented Poly(Ester-Urethane) Film with High Grafting Density for Biomedical Purpose. *Polymers* **2018**, *10*, 1–13.
- (46) Li, J.; Wang, S.; Nagai, K.; Nakagawa, T.; Mau, A. W. H. Effect of Polyethyleneglycol (PEG) on Gas Permeabilities and Permselectivities in Its Cellulose Acetate (CA) Blend Membranes. *J. Membr. Sci.* **1998**, *138*, 143–152.
- (47) Talakesh, M. M.; Sadeghi, M.; Chenar, M. P.; Khosravi, A. Gas Separation Properties of Poly(Ethylene Glycol)/Poly(Tetramethylene Glycol) Based Polyurethane Membranes. *J. Membr. Sci.* **2012**, *415–416*, 469–477.
- (48) Azizi, N.; Mohammadi, T.; Behbahani, R. M. Synthesis of a New Nanocomposite Membrane (PEBAX-1074/PEG-400/TiO<sub>2</sub>) in Order to Separate CO<sub>2</sub> from CH<sub>4</sub>. *J. Nat. Gas Sci. Eng.* **2017**, *37*, 39–51.
- (49) Brunetti, A.; Scura, F.; Barbieri, G.; Drioli, E. Membrane Technologies for CO<sub>2</sub> Separation. *J. Membr. Sci.* **2010**, *359*, 115–125.
- (50) Chatterjee, G.; Houde, A. A.; Stern, S. A. Poly(Ether Urethane) and Poly(Ether Urethane Urea) Membranes with High H<sub>2</sub>S/CH<sub>4</sub> Selectivity. *J. Membr. Sci.* **1997**, *135*, 99–106.
- (51) Yu, Y.; Ma, Y.; Yin, J.; Zhang, C.; Feng, G.; Zhang, Y.; Meng, J. Tuning the Micro-Phase Separation of the PES-g-PEG Comb-like Copolymer Membrane for Efficient CO<sub>2</sub> Separation. *Sep. Purif. Technol.* **2021**, *265*, No. 118465.
- (52) Kim, D. H.; Park, M. S.; Choi, Y.; Lee, K. B.; Kim, J. H. Synthesis of PVA-g-POEM Graft Copolymers and Their Use in Highly Permeable Thin Film Composite Membranes. *Chem. Eng. J.* **2018**, *346*, 739–747.
- (53) Kim, N. U.; Park, J.; Lee, J. H.; Kim, J. H. High-Performance Ultrathin Mixed-Matrix Membranes Based on an Adhesive PGMA-Co-POEM Comb-like Copolymer for CO<sub>2</sub> Capture. *J. Mater. Chem. A* **2019**, *7*, 14723–14731.
- (54) Lim, J. Y.; Lee, J. H.; Park, M. S.; Kim, J. H.; Kim, J. H. Hybrid Membranes Based on Ionic-Liquid-Functionalized Poly(Vinyl Benzene Chloride) Beads for CO<sub>2</sub> Capture. *J. Membr. Sci.* **2019**, *572*, 365–373.
- (55) Patel, R.; Kim, S. J.; Roh, D. K.; Kim, J. H. Synthesis of Amphiphilic PCZ-r-PEG Nanostructural Copolymers and Their Use in CO<sub>2</sub>/N<sub>2</sub> Separation Membranes. *Chem. Eng. J.* **2014**, *254*, 46–53.
- (56) Hossain, I.; Al Munsur, A. Z.; Choi, O.; Kim, T. H. Bisimidazolium PEG-Mediated Crosslinked 6FDA-Durene Polyimide Membranes for CO<sub>2</sub> Separation. *Sep. Purif. Technol.* **2019**, *224*, 180–188.
- (57) Kwisnek, L.; Heinz, S.; Wiggins, J. S.; Nazarenko, S. Multifunctional Thiols as Additives in UV-Cured PEG-Diacrylate Membranes for CO<sub>2</sub> Separation. *J. Membr. Sci.* **2011**, *369*, 429–436.